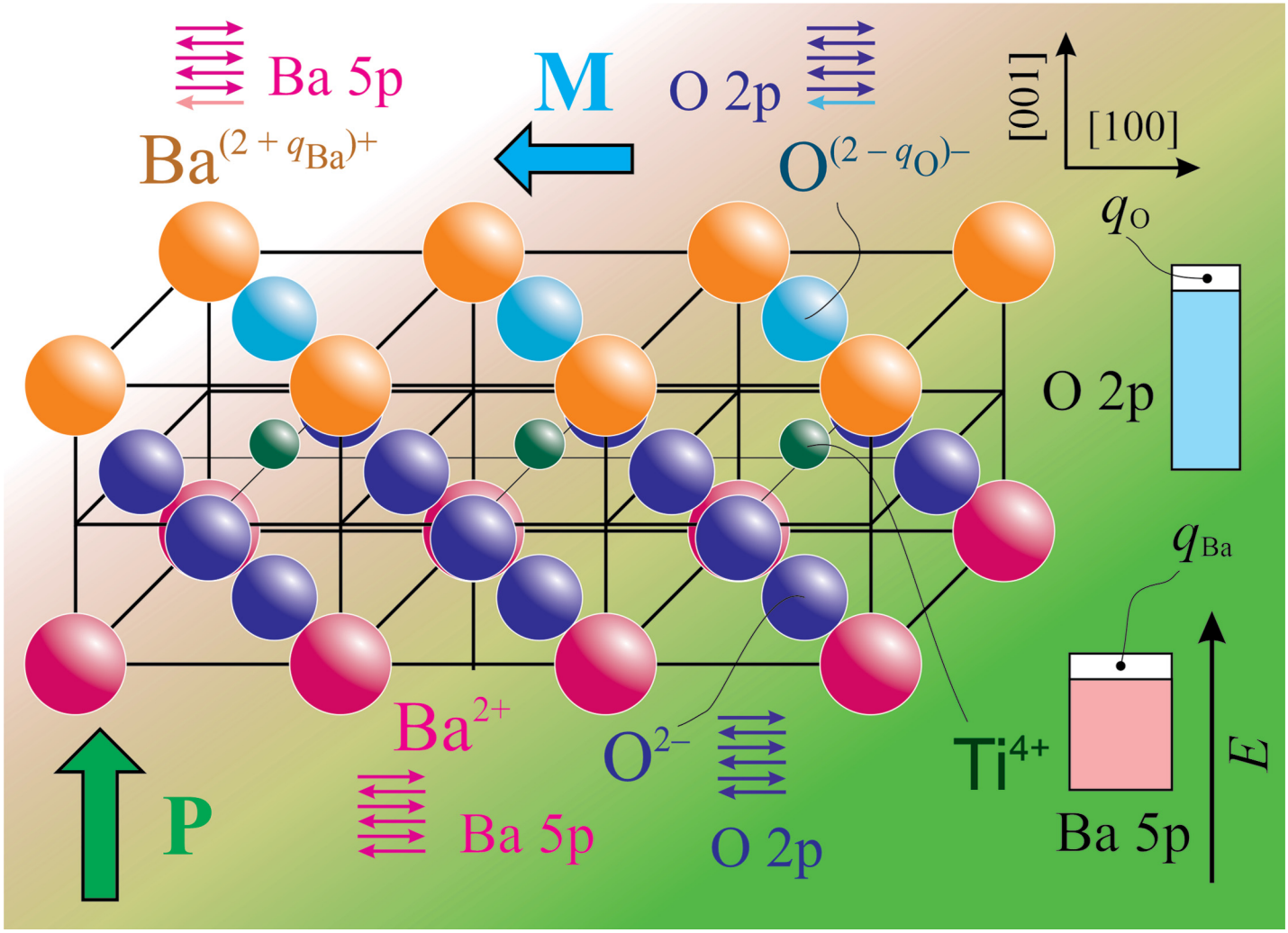

Showcasing research from Dr Cristian M. Teodorescu's laboratory, Surfaces and Interfaces, National Institute of Materials Physics, Măgurele, Romania.

Surface spin asymmetry of O 2p and Ba 5p states in $BaTiO_3$(001)

In its ferroelectric state, (001) oriented barium titanate with BaO termination features an electronic reconstruction with the surface layer positively charged. This positive charge is distributed almost evenly on the surface of Ba and O ions, yielding partially filled Ba 5p and O 2p orbitals. These orbitals feature uncompensated spins, enabling the formation of a detectable spin asymmetry. The fact that holes are stabilized on Ba 5p states, which are lower in energy than occupied O 2p states, may be regarded as a permanent population inversion induced by the ferroelectric state.

Image reproduced by permission of Cristian M. Teodorescu from *Mater. Adv.*, 2025, **6**, 8907.

As featured in:

See Cristian M. Teodorescu *et al.*, *Mater. Adv.*, 2025, **6**, 8907.

ROYAL SOCIETY OF CHEMISTRY

rsc.li/materials-advances

Registered charity number: 207890

Materials Advances

ROYAL SOCIETY OF CHEMISTRY

PAPER

View Article Online
View Journal | View Issue

Cite this: *Mater. Adv.*, 2025, **6**, 8907

Surface spin asymmetry of O 2p and Ba 5p states in $BaTiO_3$(001)

Larisa E. Borcan,[ab] Alexandru-Cristi Iancu,[ab] Nicoleta G. Apostol,[a] Adela Nicolaev[a] and Cristian M. Teodorescu *[a]

Received 14th April 2025,
Accepted 28th August 2025

DOI: 10.1039/d5ma00363f

rsc.li/materials-advances

Spin asymmetry is detected in both O 2p and Ba 5p valence states of a 12.5 nm thick (001) ferroelectric barium titanate single crystal thin film, BaO terminated, with outwards polarization. Although the occurrence of spin asymmetry in O 2p states is understandable and may be related to the surface charging of the outer layer, which induces a spin imbalance of surface oxygens, the observed spin asymmetry in deeper Ba 5p states, while still having electrons occupying states of lower binding energy, is less intuitive. This phenomenon may be explained by taking into account chemical shifts and crystal field effects together in the presence of surface charges on the surface BaO layer. In the roughest approximation, any additional positive charge is distributed equally on surface Ba and O atoms. The overall surface charge density is quite similar to the estimated value of the polarization.

1. Introduction

Multiferroicity, *i.e.*, ferroelectricity occurring together with ferromagnetism, is a rather rarely encountered phenomenon, due to fundamental considerations of electronic configurations. For the occurrence of ferromagnetism, the constituent atoms must have unoccupied orbitals with a non-zero total spin moment. For ferroelectricity, the compounds must be ionic, with cations in their maximum positive ionization state and anions in their maximum negative ionization state. Therefore, in a first approximation the electronic orbitals of all constituent atoms of a ferroelectric material are complete (fully occupied), with no net atomic spin moment.

Barium titanate $Ba^{2+}Ti^{4+}O^{2-}{}_3$ is a ferroelectric prototype, a serious candidate for many applications, because it is inexpensive and non-toxic. There are some studies in the literature on barium titanate nanocrystal systems that exhibit ferromagnetism, in addition to ferroelectricity, which is easy to understand. Generally, ferromagnetism is believed to be caused by oxygen vacancies on the surfaces of the nanoparticles.[1,2] A higher magnetization was reported for smaller nanoparticles (for example, 40 nm *vs.* 300 nm).[3] Each oxygen vacancy populates the Ti 3d states of the adjacent cations with up to 2 electrons, and these cations have parallel spins in the ferromagnetic state (and antiparallel in the antiferromagnetic state), but the former state is lower in energy. Another study showed that magnetization is proportional to the relative area of the nanoparticles.[4] The reduction of Ti^{3+} to Ti^{2+} when the concentration of oxygen vacancies increases leads to a decrease in magnetization, because Ti^{2+} is a diamagnetic impurity if the 4s electron spins are antiparallel. Other studies linked the occurrence of ferromagnetism to charge transfer in the electronic states of titanium.[5] At the same time, the occurrence of reduced oxidation states of titanium is rarely directly quantified, even though they are easy to detect using photoelectron spectroscopy, as in the case of UV-irradiated $BaTiO_3$ nanoparticles.[6]

Until now, no spin-resolved photoelectron spectroscopy study has been published for any ferroelectric material. Our group recently discovered the spin asymmetry in O 2p states in strontium titanate $SrTiO_3$(001)[7] and $SrTiO_3$(011).[8] The mechanism responsible for the occurrence of spin moments and their ferromagnetic ordering is related to surface oxygen which is in lower negative ionization states. Consequently, O 2p states could present unpaired spin electrons that align ferromagnetically. In the case of $SrTiO_3$(001), the spin asymmetry occurs simultaneously with the Ti^{3+} states and with a density of states localized in the electronic band gap, originating from partially occupied Ti 3d orbitals. Although these in-gap states themselves do not exhibit spin asymmetry, it is assumed that they involve strongly delocalized electrons in the crystal, which can mediate the interaction between oxygen moments through indirect exchange.[7] For $SrTiO_3$(011), comparing the chemical shifts from photoelectron spectroscopy and the values of spin asymmetry, it can be deduced that the surface oxygen atoms are in electronic states close to neutral oxygen (on average $O^{0.5-}$), in order to counteract Tasker's instability criterion for this surface.[9] Therefore, the atomic spin moment could be

[a] National Institute of Materials Physics, Atomiştilor 405A, 077125 Măgurele, Ilfov, Romania. E-mail: teodorescu@infim.ro
[b] University of Bucharest, Faculty of Physics, Atomiştilor 405, 077125 Măgurele, Ilfov, Romania

considerable. These considerable magnetic moments are likely ordered by direct interactions, as no evidence for Ti^{3+} or in-gap states has been observed in this case.

In this work, we extend these investigations for ferroelectric $BaTiO_3(001)$, where surfaces or outer atomic layers may be charged due to the ferroelectricity. These surfaces will be characterized by low energy electron diffraction (LEED), by core level X-ray photoelectron spectroscopy (XPS) and by spin-resolved photoelectron spectroscopy of the valence states.

2. Experimental

General aspects

The experiments were performed in the CoSMoS (combined spectroscopy and microscopy on surfaces) setup connected to the SuperESCA beamline at the Elettra storage ring facility, which operates in low 10^{-10} hPa vacuum and comprises: (i) the photoemission analysis chamber, equipped with a 5 axis sample manipulator with possibilities of heating up to 1400 K by electron bombardment and cooling down close to liquid N_2 temperature (77 K). Photoelectrons are detected with a 150 mm radius hemispherical energy analyzer (Phoibos 150, Specs) which incorporates also a mini-Mott spin detector using a Th target; (ii) the molecular beam epitaxy chamber, with a 5-axis sample manipulator, LEED and Auger electron spectroscopy, thickness monitor, several evaporators; (iii) a scanning tunneling microscopy (Aarhus 150, Specs) chamber; (iv) the storage chamber, with e-bombardment heating possibility on one port; (v) the load-lock chamber. The beamline produces photons with horizontal linear polarization in the energy range 100–1200 eV, with a typical maximum of 10^{13} photons per s at 400 eV and energy resolution in the range of 10 000. The sample plane is vertical, and the angle between the direction of the incoming X-rays and that of the electron energy analyzer is 90°, hence the direction of the emitted electrons is the same as that of the polarization of incoming X-rays. The linear polarization of incoming photons rules out spurious spin asymmetry effects related to circular polarization; also, the fact that we will later assume that the spin polarization is mainly related to the surface BaO layer excludes spin-dependent scattering processes.[10]

Sample preparation

$BaTiO_3(001)$ thin films were grown on 0.5% Nb-doped $SrTiO_3(001)$ (STON) by pulsed laser deposition (PLD) in a Surface setup, using a KrF laser (248 nm wavelength) with a repetition rate of 5 Hz and laser fluence of 1.5 J cm^{-2}. The substrate was heated at 700 °C and the partial O_2 pressure was 14 Pa. After deposition, the sample was cooled down in a rich O_2 atmosphere, of 0.1 MPa, with a rate of 10 °C min^{-1}. The film investigated in this work was the same as that used in adsorption/desorption experiments of CO,[11] CO_2[12] and C_2H_4.[13] In ref. 11, the X-ray diffraction and X-ray reflectivity of this sample are presented, and a film thickness of 12.5 nm was derived together with lattice parameters of a = 3.905 Å (in plane) and c = 4.121 Å (out-of-plane, *i.e.* along the [001] direction). Also, repeated follow-ups of the core level evolution with sample heating provided a clear shift towards lower binding energy when the temperature is increased above the Curie temperature, hence at room temperature the $BaTiO_3(001)$ is ferroelectric with its polarization oriented outwards.[14–16] The sample was quite stable under repeated adsorption/desorption cycles of several molecules, and also under repeated preparations using the procedure described below.

The $BaTiO_3(001)$ thin film was prepared firstly in the analysis chamber by annealing in oxygen to remove surface carbon ($P[O_2] \approx 5 \times 10^{-7}$ hPa). The annealing was carried out in several steps, the most severe involving a filament current of 2.7 A, an accelerating voltage of 300 V, and an emission current of approximately 30 mA. The maximum sample temperature reached was 1054 K, as measured with an optical pyrometer. During the annealing, time-resolved XPS spectra were used to monitor the carbon contamination. When the C 1s peak disappeared, the annealing was stopped and the sample was cooled down for about 10 minutes in $P[O_2] \approx 2 \times 10^{-6}$ hPa. XPS core-level measurements were then recorded. (A non-vanishing C 1s signal was nevertheless observed in a series of XPS spectra recorded with better statistics than the rapid time-resolved scans. The contamination level remained quite low, and will be discussed in detail later on.) A second annealing process was performed in the MBE under the same conditions as above, in order to minimize potential contamination of the sample during the transfer from the analysis chamber to the chamber containing the LEED system. LEED images at different electron kinetic energies are presented in Fig. 1. Back in the analysis chamber, XPS core-level measurements were repeated (Fig. 2). The sample was magnetized in two opposite directions (M1 and M2), and after each magnetization, spin-resolved measurements were performed (see Fig. 3 and 4). In the SI, more details are given about the magnetization procedures (S1). It turned out that, no matter which was the initial magnetization direction, the important parameter defining the magnetization is the stray magnetic field experienced by the sample before its introduction in the photoemission chamber, which is screened by mu-metal. In summary, these two experiments, despite the opposite directions of the strong magnetic field applied initially, were performed on samples which experienced a similar magnetic field (whose in-plane component was about 40 A m^{-1}) before getting into a magnetically screened environment. A similar magnetization procedure was applied and commented on in ref. 17.

A third magnetization experiment (M3, see SI–S2) was performed by using an electromagnet for *in situ* application of a magnetic field of similar magnitude as the stray magnetic field determined for M1, 2.

Measurements

LEED measurements were performed using a Specs rear view ErLEED 150 system located in the MBE chamber. The sample position during LEED with respect to its position during photoemission experiments is rotated by 145° clockwise. XPS

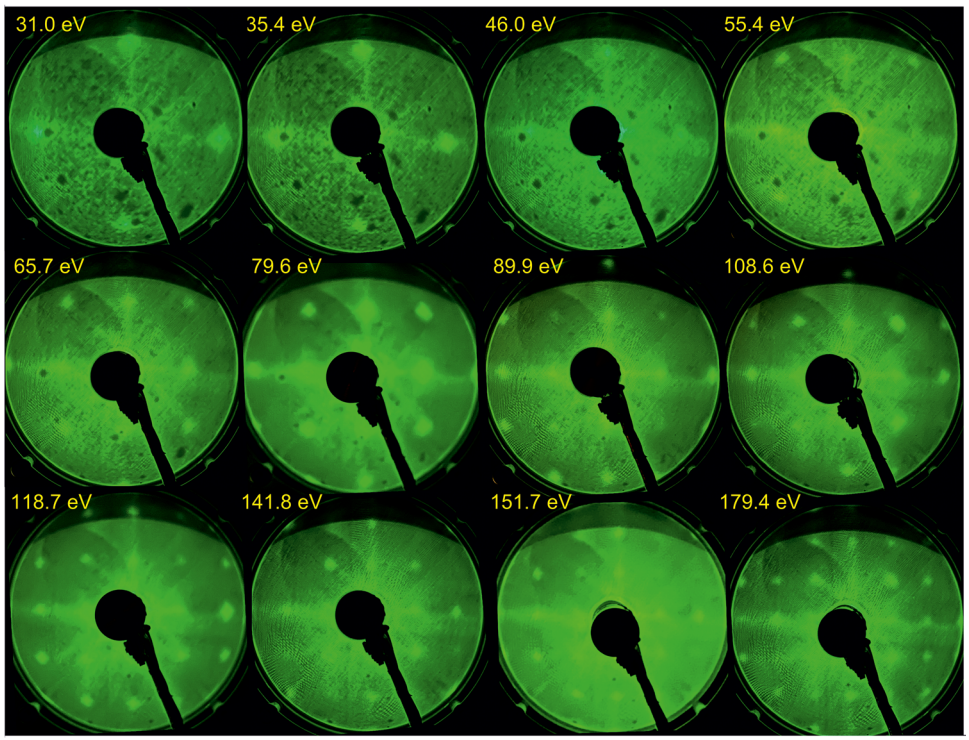

Fig. 1 Low-energy electron diffraction (LEED) images of $BaTiO_3$(001), after preparation under ultra-high vacuum conditions. Each image indicates the kinetic energy of the electrons.

and spin-resolved photoemission measurements were performed with an angular acceptance of $\pm 7^\circ$.

XPS spectra are recorded using 650 eV photon energy for survey scans, Ti 2p, O 1s and Ba 4d (analyzer pass energy: 10 eV), 390 eV (pass energy: 5 eV) for C 1s and Ba 4d, and 260 eV for the valence band (pass energy: 10 eV). The inelastic mean free path is similar for all core levels investigated. No charging effects were observed as confirmed by monitoring the evolution of quickly acquired individual scans.

The spin-resolved measurements are obtained with linearly *p*-polarized 105 eV photon energy. The acceleration voltage of the Mott detector was 25 kV, and in these conditions the Sherman function provided by the manufacturer is SF $\approx$ 0.12.[18] The recalibration of the spin channels is explained in detail in ref. 8 and 17 and it comprises a linear transformation of spectra such that their intensity becomes similar in the regions at the very beginning and at the very end of the spectrum. The surface Brillouin zone explored during the measurement is within a reasonable approximation the same as outlined in ref. 7, *i.e.* it encompasses with a good approximation the whole area of a surface Brillouin zone. In other words, this ensures that the measured spectra can be related to the angle-integrated density of states of the material. The total spin-resolved acquisition time implied 8 scans, each lasting $\sim$46 minutes (368 minutes in total). The vacuum level in the analysis chamber was a high 10^{-10} hPa for the M1, 2 experiments and low 10^{-10} hPa for the M3 experiment, and this manifests in a considerably lower contamination of the $BaTiO_3$(001) surface in this last experiment.

3. Results

Low energy electron diffraction

Fig. 1 presents low energy-electron diffraction (LEED) images obtained at different kinetic energies of the incident electrons. The energies at which constructive (in phase) or destructive (out of phase) interference of the electron waves associated with reflection on surfaces separated by a monoatomic terrace d_{lmn}, are deduced based on the formalism developed in ref. 8.

The electron kinetic energy is expressed as:

$$E_K\,[\mathrm{eV}] \approx 3.8105k^2\,[\mathrm{\AA}^{-1}] \quad (1)$$

where $k = 2\pi/\lambda$ is the electron wavevector, λ is the associated wavelength, and the path difference in electron diffraction on the two surfaces is considered equal to an integer number of half wavelengths, p (even for constructive interference and odd for destructive interference). Two hypotheses are considered:

(a) If the path difference between electrons reflected normally on the surface is an integer number of wavelengths, the interference is constructive.[19] If it is a half-integer number of wavelengths, the interference is destructive. If d_{lmn} is the dimension of a terrace in the [*lmn*] direction normal to the surface, the conditions for constructive/destructive interference are with constructive interference if p is even and destructive if p is odd.

$$2d_{lmn} = p\lambda/2 \text{ or } 2kd_{lmn} = p\pi \quad (2)$$

(b) A more refined model is presented in ref. 8. The diffraction angle, α, is taken into account. The condition for

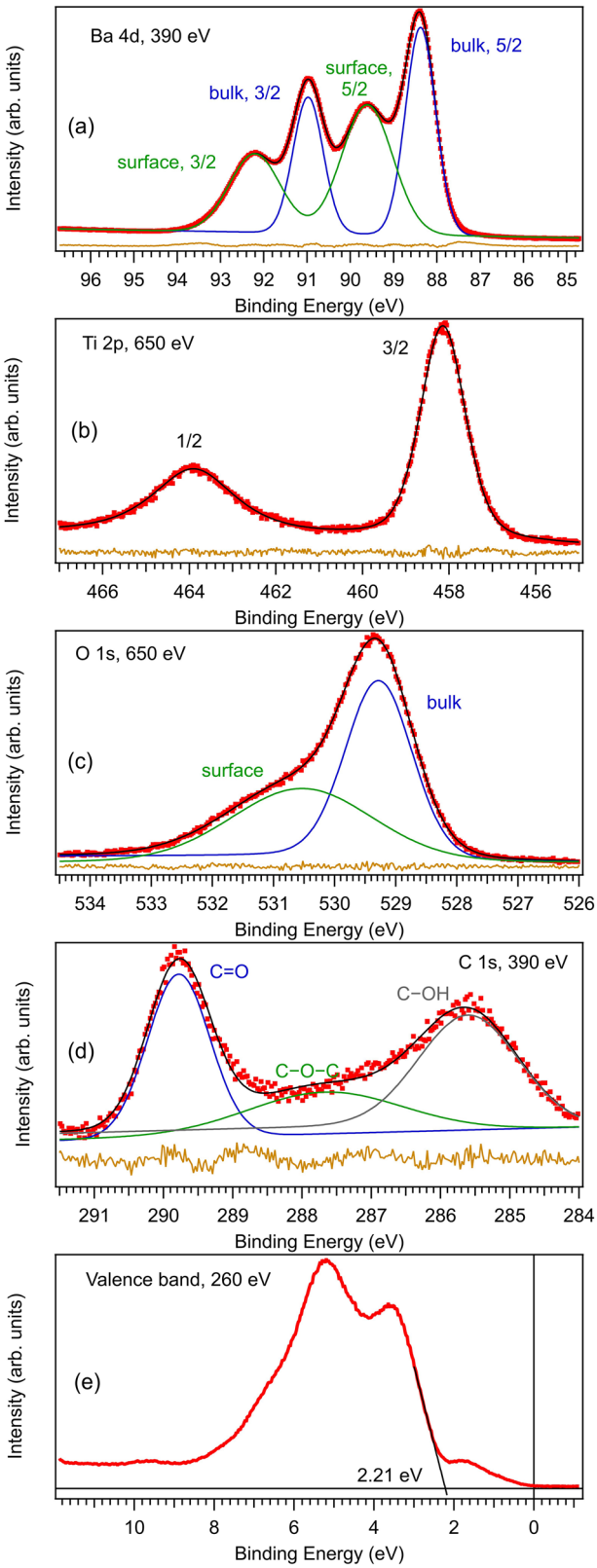

Fig. 2 Results obtained using core-level photoelectron spectroscopy on $BaTiO_3$(001). (a) The Ba 4d spectrum, with an excitation energy of 390 eV. (b) The Ti 2p spectrum, with an excitation energy of 650 eV. (c) The O 1s spectrum, with an excitation energy of 650 eV. (d) The C 1s spectrum, with an excitation energy of 390 eV. (e) Valence band spectrum, with an excitation energy of 260 eV. For (a)–(d) the 'deconvolutions' of the spectra are also shown, with blue, green and gray curves. The brown curves represent the residuals.

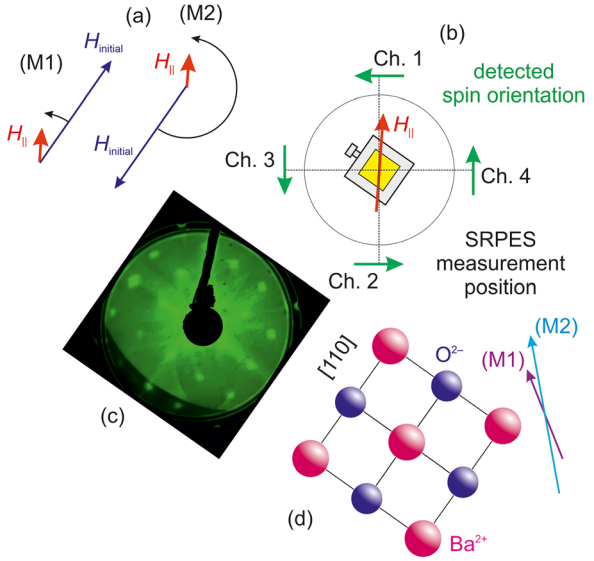

Fig. 3 Magnetization geometry and sample orientation for different analyses. (a) The orientation of the initially applied magnetic field, as well as its rotation relative to the sample until its introduction into the analysis chamber, which is shielded from external magnetic fields by using mu-metal. (b) The sample orientation during the photoelectron spectroscopy (PES) measurements, along with the final orientation of the magnetic field applied in the sample plane before transferring it to the analysis chamber, and the configuration of the spin-resolved detection channels together with the spin direction recorded by each channel. (c) An LEED image from Fig. 1, rotated to match the sample position during the photoelectron spectroscopy measurements. (d) A schematic of the orientation of the first BaO crystalline plane during the measurements, along with the sample magnetizations inferred from the spin-resolved photoelectron spectroscopy (Fig. 4).

constructive/destructive interference becomes $d_{lmn}(1 + \cos\alpha) = p\lambda/2$, thus $kd_{lmn}(1 + \cos\alpha) = p\pi$. Taking into account the diffraction condition for the appearance of LEED spots, $a_{ijk}\sin\alpha = \lambda$, where a_{ijk} is the interatomic distance in the [ijk] in-plane direction, and replacing the value of α we obtain:

$$k = \frac{2\pi d_{lmn}}{p}\left[\left(\frac{p}{2d_{lmn}}\right)^2 + \frac{1}{a_{ijk}^2}\right] \quad (3)$$

The wave vector values are calculated under hypothesis (a), eqn (2) or hypothesis (b), eqn (3), and then the corresponding values of the electrons' kinetic energy are derived using eqn (1). The resulted values are presented in Table 1.

One may observe that for any of the energies corresponding to the out-of-phase condition we did not identify any extinction of the LEED maxima, meaning that the termination of $BaTiO_3$(001) is uniform across the entire analyzed area (there are no monoatomic terraces). This indicates that the layer is either terminated in BaO or TiO_2.

X-ray photoelectron spectroscopy

The XPS spectra are shown in Fig. 2. The Ti 2p spectrum (Fig. 2(b)) is fitted by using one component (Ti^{4+}), indicating that titanium sub-oxides (titanium in reduced states) are absent, and that titanium is not present in the surface layer.

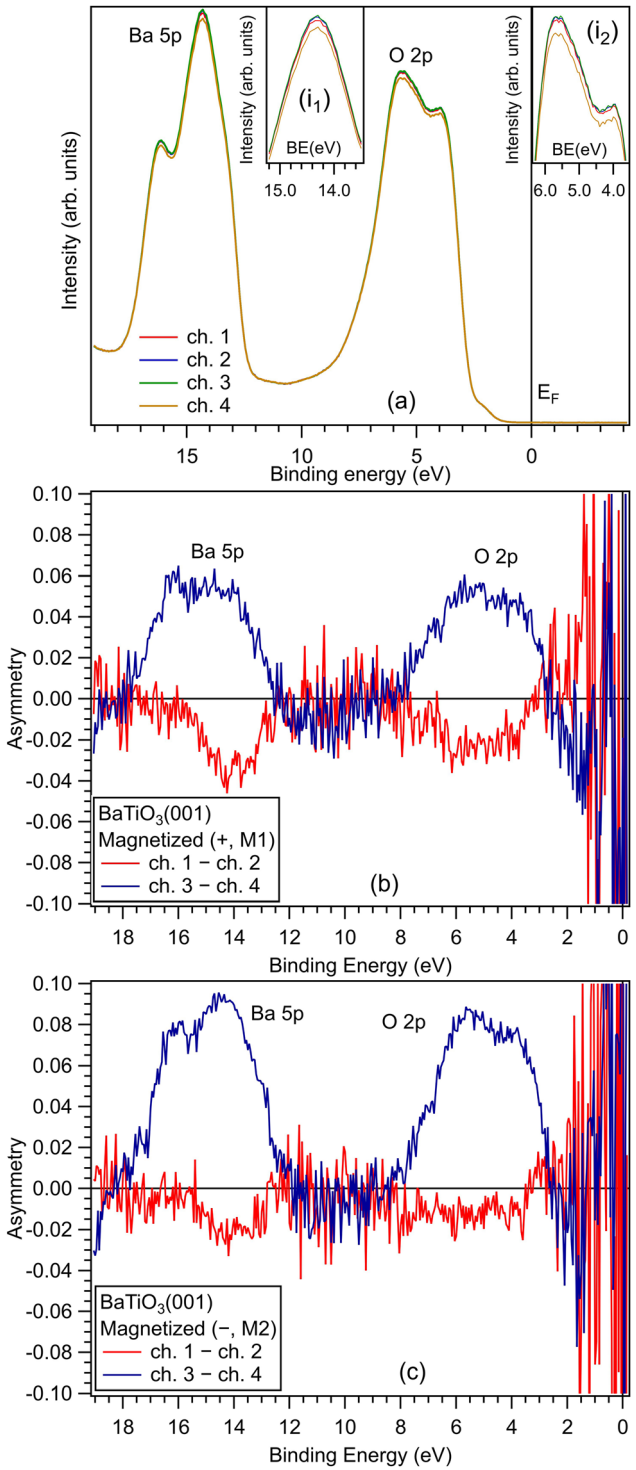

Fig. 4 Valence band spin-resolved photoelectron spectroscopy, obtained with a photon energy of 105 eV. (a) Signals obtained for the different spin-resolved channels (Fig. 3(b)). Insets (i_1) and (i_2) are magnified areas of the maxima corresponding to Ba 5p and O 2p states, respectively. (b) and (c) show the spin asymmetry detected for the sample subject to the M1 or M2 magnetization process, as represented in Fig. 3(a).

On the other hand, the Ba 4d spectrum (Fig. 2(a)) and the O 1s spectrum (Fig. 2(c)) show two components: one for the bulk and one for the surface, the latter at higher binding energy. Thus,

Table 1 Energies for which the in-phase or out-of-phase LEED conditions are realized on $BaTiO_3$(001). The first column represents the number of half wavelengths in the path difference, the second column represents the application of the simplified condition defined by eqn (2), and third and fourth columns represent the more refined model, eqn (3), using the in plane direction [110]. The values from the parenthesis are the experimental registered values of the LEED diffraction, see Fig. 1

p	E_K [eV], eqn (2)	E_K [eV], eqn (3)	Condition
3	19.93 (—)	31.02 (31.0)	Out-of-phase
4	35.43 (35.4)	45.98 (46.0)	In-phase
5	55.36 (55.4)	65.67 (65.7)	Out-of-phase
6	79.72 (79.6)	89.89 (89.9)	In-phase
7	108.51 (108.6)	118.60 (118.7)	Out-of-phase
8	141.73 (141.8)	151.76 (151.7)	In-phase
9	179.37 (179.4)	189.38 (—)	Out-of-phase

the XPS spectra confirm the uniform BaO termination of $BaTiO_3$(001). (Similar arguments are discussed in more details in ref. 11–13). Also, some carbon contamination was observed (Fig. 2(d)). The total amount of carbon present in all detected states represent approximately one carbon atom for 7 BaO surface unit cells (C_{total}:$Ba_{surf.}$ = 0.144 ± 0.017). In computing these ratios, theoretical photoionization cross sections σ_{PI} and asymmetry parameters β_{PI} are used from ref. 20. One has to divide the experimental integral line amplitudes by $\sigma_{PI}(1 + \beta_{PI})$, since in our setup electrons are detected in the direction of the linear polarization of the incoming radiation. The higher binding energy components represent a few percent of monolayer contamination ($C_{C=O}$:$Ba_{surf.}$ = 0.053 ± 0.006 and C_{C-O-C}:$Ba_{surf.}$ = 0.033 ± 0.004), while the lower energy component represents a contamination of C_{C-OH}:$Ba_{surf.}$ = 0.058 ± 0.007. (In attributing the carbon components, we used ref. 21). This surface was then slightly more contaminated than the ones explored in ref. 11–13, where the initial contamination was below 0.1 monolayers. The $BaTiO_3$(001) composition, obtained through standard XPS measurements, is $BaTiO_{2.91}$,[12] indicating a detectable concentration of oxygen vacancies. The contamination level was also checked after the M1, 2 measurements which lasted more than 15 hours (see SI–S3), and the result was a slightly lower contamination with C═O and a higher contamination with carbon from lower binding energy components: $C_{C=O}$:$Ba_{surf.}$ = 0.026 ± 0.003, C_{C-O-C}:$Ba_{surf.}$ = 0.043 ± 0.006, and C_{C-OH}:$Ba_{surf.}$ = 0.099 ± 0.013. Before the M3 experiment, the sample was again prepared from the beginning (it was a different synchrotron radiation run) and the contamination level was significantly lower (see SI–S4): $C_{C=O}$:$Ba_{surf.}$ = 0.014 ± 0.001, C_{C-O-C}:$Ba_{surf.}$ = 0.007 ± 0.001, and C_{C-OH}:$Ba_{surf.}$ = 0.023 ± 0.002. Unfortunately, for this last experiment the spin detectors had a lower efficiency, therefore the spin-resolved spectra are of lower quality. We will discuss also these data, but the main considerations regarding the spin asymmetry will rely mainly on the M1, 2 experiments.

The XPS spectra were 'deconvoluted' by using Gaussian profiles for Ba 4d and C 1s, and Voigt profiles[22] for Ti 2p and O 1s. For Ti 2p, the two lines of the doublet exhibit different Lorentzian widths due to the shorter lifetime of the $2p_{1/2}$ vacancy as compared to $2p_{3/2}$, which is caused by adjacent

Table 2 Values obtained from the spectra 'deconvolution' in Fig. 2. W represents the full width at half-maximum (FWHM) of the Gaussian lines for Ba 4d and C 1s. For the Ti 2p and O 1s spectra Voigt lines[22] were used, in this case Gaussian widths (WGauss) and Lorentzian widths (WLor) are distinguished. For Ti 2p the two lines of the 2p doublet have different Lorentzian widths, due to Coster–Kronig deexcitation processes that are leading to a shorter lifetime for $2p_{1/2}$ compared to $2p_{3/2}$. SOS represents the spin–orbit splitting, BR is the branching ratio defined as the ratio of the intensities of the two lines of a doublet, BE[1, 2, ...] are the binding energies of the lines (of the lowest binding energy one for doublets), A[1, 2, ...] are the integral amplitudes of the peaks, and b[1, 2, ...] is the coefficient corresponding to the inelastic scattering background. Photon energies are mentioned in parentheses in the first line of the table. Error bars are not added, to avoid overcrowding, but they were taken into account when evaluating the composition or contamination from line integral amplitudes

Ba 4d (390 eV)		Ti 2p (650 eV)		O 1s (650 eV)		C 1s (390 eV)	
Parameter	Value	Parameter	Value	Parameter	Value	Parameter	Value
W1 (eV)	0.820	WLor1(3/2) (eV)	0.462	WLor (eV)	0.121	W1 (eV)	1.059
SOS1 (eV)	2.599	WLor2(1/2) (eV)	1.908	WGauss1 (eV)	1.236	BE1 (eV)	289.780
BR1	1.526	WGauss1 (eV)	0.964	BE1 (eV)	529.276	A1 (arb.)	984
BE1 (eV)	88.379	SOS (eV)	5.754	A1 (arb.)	1355	b1	0.000
A1 (arb.)	19624	BR	1.418	b1	0.031	W2 (eV)	2.627
b1	0.000	BE (eV)	458.145	WGauss2 (eV)	2.658	BE2 (eV)	287.658
W2 (eV)	1.389	A (arb.)	1606	BE2 (eV)	530.534	A2 (arb.)	613
SOS2 (eV)	2.598	b	0.004	A2 (arb.)	1166	b2	0.006
BR2	1.648					W3 (eV)	1.703
BE2 (eV)	89.611					BE3 (eV)	285.586
A2 (arb.)	20120					A3 (arb.)	1075
b2	0.000					b3	0.019

Coster–Kronig deexcitation channels emitting electrons from the valence band.[23]

Additionally, the coefficient corresponding to the inelastic electron scattering background is zero (or very low) for the components arising from atoms in the first surface layer.[24] The fitting ('deconvolution') parameters are given in Table 2. The fact that the branching ratio of Ti 2p is considerably lower than its theoretical value of 2 is due to the selective scattering of outgoing electrons from Ti 2p orbitals with high angular momenta on the oxygen anions situated on top of the titanium, which eliminates them from the flux of the detected photoelectron. Ref. 11 provides greater detail of this observation.

The overall conclusion of the XPS data is the good sample stoichiometry, the presence of some oxygen vacancies and its BaO termination, together with results obtained from previous experiments related to its outwards polarization. In the SI, S3 and S4 present also the results of the 'deconvolution' of the XPS spectra recorded after the M1, 2 experiments and before the M3 experiment. Slight deviations in the Ba 4d, Ti 2p and O 2p binding energies can be attributed to different levels of contamination.[11–13] The binding energies of the surface components of Ba and O are lower by about 0.08 eV and 0.1 eV for the ''contaminated'' sample (measurements after M1 + M2 magnetization and spin-resolved acquisitions), which may be explained by a lower downwards surface band bending in the presence of external sources of stabilizing charges.[16,25] Contamination issues and possible effects on the spin asymmetry will be discussed in a later subsection.

Spin-resolved photoelectron spectroscopy

Next, we present the results of the spin-resolution photoelectron spectroscopy measurements. Fig. 3 shows the geometry of magnetization and the measurement setup for the sample, resulting from the sketch for the M1, 2 experiments presented in the SI–S1). Two *in situ* magnetization procedures where performed on the sample after preparation, which are explained in detail in ref. 17. In both cases, the sample's magnetization alignment, just before being introduced into the photoelectron spectroscopy analysis chamber (magnetically shielded by mu-metal), was the same, but initially a stronger magnetic field was applied and was rotated relative to the sample, as in Fig. 3(a). The orientation of the different spin-detection channels is shown in Fig. 3(b), and the sample orientation (along with the corresponding LEED image) is shown in Fig. 3(c and d). From the analysis of the spin asymmetry signal, the relative orientation of the sample magnetization in both magnetization cases, as shown in Fig. 3(d), was determined. To a good approximation, the sample magnetization lies along the [100] in-plane direction.

In Fig. 4, the spin-resolved photoelectron spectroscopy results are represented. The detection channels for different spins alignments were normalized following the procedure described in ref. 7, 8 and 17. A spin asymmetry $(I_+-I_-)/(I_++I_-)$/SF is observed not only for the O 2p states, as in the case of strontium titanate,[7,8] but also for the Ba 5p states, which exhibit a considerably higher binding energy.[26] While for the O 2p case we can presume that some intensity in the density of states originates from the Ti 3d signal, it is hard to propose such a mechanism for the Ba 5p case. These spin asymmetry signals suggest that the surface oxygen is in a lower negative ionization state ($O^{\eta-}$, $\eta < 2$), a process similar to that detected in strontium titanate.[7,8] However, the results suggest that the surface barium is in a higher-than 2 ionization state, $Ba^{\gamma+}$, $\gamma > 2$, in order to obtain a net spin moment on the Ba 5p states.

Overall, it seems that $BaTiO_3(001)$ presents a strong electronic surface reconstruction, with the first $Ba^{\gamma+}O^{\eta-}$ layer being considerably charged ($(\gamma-\eta > 0$) and, probably, compensation charges are distributed in the underlying layers to stabilize the ferroelectric state.[25]

The results of the spin-resolved measurements after applying a magnetic field on the sample by using an electromagnet (M3) are presented in the SI–S5. We already mentioned that the contamination of this sample was significantly lower, C_{total}:$Ba_{surf.}$ = 0.043 ± 0.004, which means in average one carbon atom for ~23 BaO surface unit cells. Despite the cleaner sample, the statistics of the spin-resolved data is worse than for those presented in Fig. 4, owing to a significant decrease of the efficiency of the spin channeltrons: nevertheless, one readily identifies a spin asymmetry with intensity similar to that of the M1 experiment. These data will, nevertheless, be included in a later discussion.

4. Discussion

Ferroelectricity-induced permanent inversion of population and related spin asymmetry

The result with spin asymmetry detected in both O 2p and Ba 5p bands is somehow puzzling. In a purely ionic model of the compound $Ba^{2+}Ti^{4+}O^{2-}_3$ the last occupied states originate from O 2p orbitals. If these orbitals are completely occupied, their spin configuration (↑↓↑↓↑↓) implies no net spin moment able to become long-range ordered. As soon as one supposes that these orbitals are not completely filled, some spin imbalance occurs and eventually the atomic oxygen spin can feature long-range ordering. This is valid in particular for $SrTiO_3$(011) where the successive atomic layers O_2 and SrTiO are charged (∓4 in the purely ionic model). Since this succession of charged layers yields an infinite potential energy inside the sample, (at least) the surface layers should feature a different charge state.[9] If the last atomic layer is O_2, then these oxygens show a charge state different from (–2 for each oxygen), then from these orbitals some spin imbalance shows up.[8] The same surface positive charging occurs also for $SrTiO_3$(001), though to a lower extent.[7] To summarize, surface charging should yield some electron depletion in the highest occupied band, which is the O 2p band.

But in the actual case one detects spin asymmetry in both O 2p and Ba 5p states, the latter with larger binding energy, despite the fact that most of the O 2p states, sitting energetically above the Ba 5p states, should retain a high electron population. Naively, one should suppose that all holes related to missing electrons should be located at the top of the valence band, *i.e.* in the O 2p region. But we have evidence that deeper valence states (related to Ba 5p) become electron depleted, although there are still some occupied states at an energy above those free states (in the O 2p states). This is unconceivable in a simplest model where electrons should be extracted from the sample progressively with increasing binding energy. This situation resembles an inversion of population, but it is permanent and should be related to the ferroelectricity of the material. In the following, we shall give an estimate of the reasons for this phenomenon to happen. An estimate of chemical shifts and crystal field effects, which will be detailed below, yields to the conclusion that the state of lower total energy (highest total binding energy) is that where the charge located on the outer layer is split on surface oxygen and barium.

One supposes that the surface BaO unit cell has an overall charge $Q > 0$. This charge can be viewed as a ''fixed charge'' of the ferroelectric material, since it was demonstrated that the rumpling of the first BaO layer and that of the second TiO_2 layer is minimal.[27] Therefore, the only reasonable candidate for these fixed charges for outwards polarization is the overall charging of the outer BaO layer. At the same time, these ''fixed charges'' are equilibrated by ''compensating''[28] or ''stabilizing''[25] charges of opposite sign in the next layers of the material, such that the internal field in the material vanishes. The fact that the outer layer is positively charged has a direct effect on the occurrence of the spin asymmetry in the O 2p band, as demonstrated also for $SrTiO_3$(001)[7] and especially for $SrTiO_3$(011).[8] As commented above, the additional effect in the case of $BaTiO_3$(001) is the observed spin asymmetry also in the deeper Ba 5p band, which means that also this band is incompletely occupied.

We proceed now with the estimate. Assume:

$$Q = q_{Ba} + q_O > 0 \quad (4)$$

the aim of the following considerations is to estimate the share of the additional charges on Ba and O, q_{Ba}, q_O out of Q. The position of the O 2p and Ba 5p energy bands in the non-ferroelectric (*i.e.* $Q = 0$) and ferroelectric case is represented in Fig. 5. Some shifts in the (median) position of the bands are taken into account when the layer becomes charged, such as: (i) $\delta_{Ba,O}$, which are chemical shifts, *i.e.* due to the different charging states of surface Ba and O: $Ba^{(2+q_{Ba})^+}$ instead of Ba^{2+}

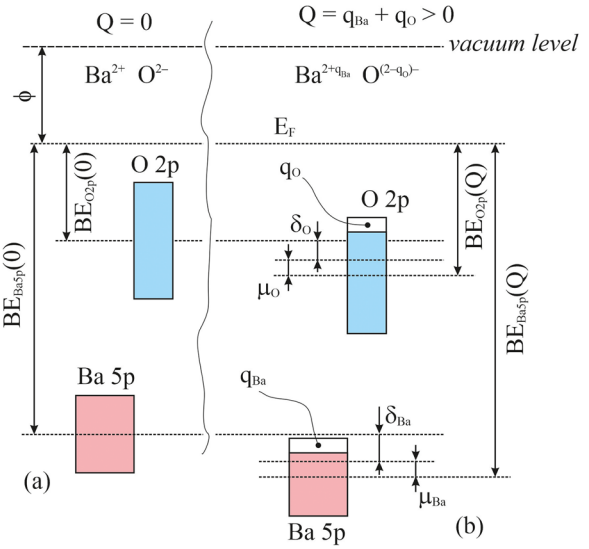

Fig. 5 (a) Position of completely filled O 2p and Ba 5p bands in a bulk $Ba^{2+}O^{2-}$ layer. (b) Position of partially filled O 2p and Ba 5p bands in a surface charged $Ba^{(2+qBa)^+}O^{(2-qO)^-}$ layer, with $q_{Ba} + q_O = Q$, the total charge per surface unit cell. $\delta_{Ba,O}$ are chemical shifts due to additional charges on each type of ion, and $\mu_{Ba,O}$ are shifts due to the surrounding crystal fields.

and $O^{(2-q_O)^-}$ instead of O^{2-}. (ii) $\mu_{Ba,O}$ are contributions from the crystal field (Madelung-like terms in two dimensions 2D). These can be expressed as:

$$\mu_{Ba} = \frac{e^2}{2\sqrt{2}\pi_0 a}\left\{ q_{Ba} \sum_{\substack{i,j=-\infty \\ i+j=2k \\ (i,j)\neq(0,0)}}^{\infty} \left(i^2+j^2\right)^{-1/2} + q_O \sum_{\substack{i,j=-\infty \\ i+j=2k+1}}^{\infty} \left(i^2+j^2\right)^{-1/2} \right\} \equiv 2\sqrt{2}\omega_0 \frac{a_B}{a}(q_{Ba}S_{2k} + q_O S_{2k+1}) \quad (5)$$

for barium, and:

$$\mu_O = 2\sqrt{2}\omega_0 \frac{a_B}{a}(q_O S_{2k} + q_{Ba} S_{2k+1}) \quad (6)$$

for oxygen. In the above equations, a_B is the Bohr radius, $\omega_0 = e^2/(8\pi\varepsilon_0 a_B)$ is the Rydberg constant, ε_0 is the vacuum permittivity, a is the in-plane lattice constant (distance between two surface bariums), and k is an integer. The definition of the 2D sums S_{2k}, S_{2k+1} is straightforward from eqn (5). These sums are infinite and one can easily understand this: for instance, in the case of an infinite 2D continuous charge distribution, the total energy experienced by a small given disk of area $\delta s_0 = \pi r_0^2$ with the rest of the charge with a surface charge density σ also diverges:

$$W = \iint \frac{\sigma^2 \delta s_0 \mathrm{d}s}{4\pi\int_0 r} = \frac{\sigma^2 \delta s_0}{2\int_0} \int_{r_0}^{\infty} \mathrm{d}r \to \infty \quad (7)$$

Nevertheless, we will demonstrate below that in the dependence of q_{Ba} and q_O of Q only the difference $S_{2k}-S_{2k+1}$ will show up, and this difference is computed numerically for increasing summation limits and is not diverging. We obtained $S_{2k}-S_{2k+1} \equiv \Delta S \approx -1.62$. At the end of this subsection, we will introduce also the ''compensating'' negative charge located on inner layers of $BaTiO_3$(001) and prove that the divergence problems are easily solved.

The total (binding) energy difference due to 2D Madelung terms is obtained by multiplication by the number of electrons on barium and oxygen, such as:

$$\Delta W_M = \mu_{Ba}(6-q_{Ba}) + \mu_O(6-q_O) = \ldots = 2\sqrt{2}\omega_0 \frac{a_B}{a} \times \left\{ 6(q_{Ba}+q_O)(S_{2k}+S_{2k+1}) - \left(q_{Ba}{}^2 S_{2k} + 2q_{Ba}q_O S_{2k+1} + q_O{}^2 S_{2k}\right)\right\} \quad (8)$$

In the following, we will note by $\tilde{w}_0 = 2\sqrt{2}\omega_0 a_B/a \approx 5.23$ eV for $a = 3.9$ Å.

We compute now the chemical shifts due to different ionic charges. For a ''test'' electron situated at the distance r from the nucleus of an atom with charge state q, the influence of the other atomic electrons can be modelled by introducing an ''effective'' positive charge experienced by the considered electron, which has to be close to the atomic number Z close to the nucleus and to $1 + q$ when the test electron is far away. A simple model for this effective charge is an exponential decay:

$$z(Z,q;r) = 1 + q + (Z-q-1)\exp\left(-\frac{r}{c}\right) \to \begin{cases} 1+q, r\to\infty \\ Z, r\to 0 \end{cases} \quad (9)$$

where c can be interpreted as a typical dimension of the atom (taking into account all electronic shells). Actually, we may apply the same model for an external electronic shell only, by considering that c is the radius of that shell (*i.e.* O 2p or Ba 5p) and Z is the charge of the atomic species without the external shell (4 for O 2p, 8 for Ba 5p). The potential energy experienced by the test electron is obtained by a series development:

$$V(r) = -\frac{z(Z,q;r)e^2}{4\pi\varepsilon_0 r} \approx -\frac{Ze^2}{4\pi\varepsilon_0 r} + \frac{(Z-q-1)e^2}{4\pi\varepsilon_0 c} \quad (10)$$

and one notices that a constant term is obtained. Hence, in the lowest order of perturbation theory, this term will represent the shift in binding energy for the atomic species in question:

$$BE \approx BE^{(0)} - \frac{(Z-q-1)e^2}{4\pi\varepsilon_0 c} \quad (11)$$

In other words, in this approximation the chemical shift varies linearly with the charge state of the atom. The change in

chemical shift due to the additional charges on barium and oxygen for the surface BaO layer can then be expressed as:

$$\delta_{Ba} \approx \left\{ BE_{Ba}^{(0)} - \frac{(Z_{Ba} - q_{Ba} - 3)e^2}{4\pi\varepsilon_0 c_{Ba}} \right\} - \left\{ BE_{Ba}^{(0)} - \frac{(Z_{Ba} - 3)e^2}{4\pi\varepsilon_0 c_{Ba}} \right\} = \frac{q_{Ba}e^2}{4\pi\varepsilon_0 c_{Ba}} \equiv w_{Ba} q_{Ba} \quad (12)$$

$$\delta_{O} \approx \left\{ BE_{O}^{(0)} - \frac{(Z_{O} - q_{O} + 1)e^2}{4\pi\varepsilon_0 c_{O}} \right\} - \left\{ BE_{O}^{(0)} - \frac{(Z_{O} + 1)e^2}{4\pi\varepsilon_0 c_{O}} \right\} = \frac{q_{O}e^2}{4\pi\varepsilon_0 c_{O}} \equiv w_{O} q_{O} \quad (13)$$

In the same way as for the contribution of the crystal field effects, one may estimate the total binding energy difference due to chemical shifts:

$$\Delta W_{CS} = \delta_{Ba}(6 - q_{Ba}) + \delta_{O}(6 - q_{O}) = 6(w_{Ba}q_{Ba} + w_{O}q_{O}) - (w_{Ba}q_{Ba}^2 + w_{O}q_{O}^2) \quad (14)$$

The total difference in binding energies is given by:

$$\Delta W = \Delta W_{M} + \Delta W_{CS} \quad (15)$$

By noting $q_{Ba} = x$ and $q_{O} = Q - x$, one obtains after some manipulations a function of second degree of the total energy as function of x:

$$\Delta W = -\{w_{Ba} + w_{O} + 2\tilde{w}_0(S_{2k} - S_{2k+1})\}x^2 + \{6(w_{Ba} - w_{O}) + 2(S_{2k} - S_{2k+1})Q\tilde{w}_0 + 2w_{O}Q\}x + \{6\tilde{w}_0 Q(S_{2k} + S_{2k+1}) - \tilde{w}_0 S_{2k} Q^2 + 6w_{O}Q - w_{O}Q^2\} \equiv A(Q)x^2 + B(Q)x + C(Q) \quad (16)$$

An estimate of the energy terms may be proposed by using ionic radii $c_{Ba} \approx 1.61$Å (Ba^{2+} with 12-fold coordination), and $c_{O} \approx 1.40$ Å (O^{2-} with 6-fold coordination).[29] It follows $w_{Ba} \approx 8.95$ eV and $w_{O} \approx 10.3$ eV. A few lines below will see that one has to impose $w_{Ba} \approx w_{O}(\sim 9.6$ eV) (average value) to get consistent results. Using $S_{2k} - S_{2k+1} \approx -1.62$, it results that $A < 0$ and then $\Delta W(x)$ is a function with a maximum. The maximum is given by:

$$x_{max.}(Q) = -\frac{B(Q)}{2A(Q)} \quad (17)$$

In order to obtain $x_{max}(0) = 0$ one needs to suppose $w_{Ba} = w_{O}$ ($=w$), as mentioned above. In this case, the result is quite simple, *i.e.* $x_{max}(Q) = Q/2$.

Experimentally, the observed asymmetry is connected to the charge of the p orbitals by $A = q/(6 - q)$, which in turn yields $q = 6A/(1 + A)$. The average asymmetries and derived charges of Ba 5p and O 2p orbitals are listed in Table 3.

It can be easily computed that the share of the total charge Q (0.274e for M1 and 0.445e for M2) located on barium ranges between 0.57 and 0.60 of the total charge Q.

Table 3 Asymmetries and derived charge states for Ba 5p and O 2p orbitals, in the two magnetization geometries

Magnetization	State	Asymmetry (%)	q
M1	Ba 5p	2.82 ± 0.50	0.164 ± 0.029
M2	Ba 5p	4.42 ± 0.69	0.254 ± 0.040
M1	O 2p	1.86 ± 0.30	0.110 ± 0.018
M2	O 2p	3.29 ± 0.45	0.191 ± 0.026

By taking into account the multitude of the approximations employed in the above evaluation, the agreement with the estimated value of $q_{Ba}/Q \approx 0.5$ is quite satisfactory.

We will now proceed to the estimate of the interaction with the ''compensating'' charge located in the inner layers of $BaTiO_3$(001). Since the Ti 2p spectrum can be fitted with a single component (Fig. 2(b)) and also no visible signs of Ti 3d states are identified in the valence band (*e.g.* in-gap states of about 1 eV binding energy, as for strontium titanate[7,8]), then we can consider that no additional electrons are located on the second TiO_2 layer of the crystal. The third (BaO) layer may accommodate some additional electrons only on barium, on Ba 5s states. These barium atoms will then have a lower binding energy, and are observed in Ba 4d XPS spectra (Fig. 2(a)). Also, a 'tail' is observed in the valence band spectra (Fig. 2(e) and 4(a)) which can be due to Ba 5s states from underlying barium (starting from the third atomic layer). Note that the relative amplitude of these 'tail' states increases when the measurement is less surface sensitive (photon energy 260 eV *vs.* 105 eV). Hence, as a first approximation we will suppose that a charge $-Q$ is distributed on each barium from the third atomic BaO shell. The Madelung term acting on surface barium from the third BaO atomic layer will be:

$$\mu'_{Ba} = -\frac{e^2 Q}{2\sqrt{2}\pi\varepsilon_0 a} \sum_{\substack{i,j=-\infty \\ i+j=2k \\ (i,j)\neq(0,0)}}^{\infty} (i^2 + j^2 + 2)^{-\frac{1}{2}} \equiv -\tilde{w}_0 Q T_{2k} \quad (18)$$

On surface oxygen:

$$\mu'_{O} = -\frac{e^2 Q}{2\sqrt{2}\pi\varepsilon_0 a} \sum_{\substack{i,j=-\infty \\ i+j=2k+1 \\ (i,j)\neq(0,0)}}^{\infty} (i^2 + j^2 + 2)^{-\frac{1}{2}} \equiv -\tilde{w}_0 Q T_{2k+1} \quad (19)$$

again, with straightforward interpretations of the (diverging) sums T_{2k} and T_{2k+1}. An additional Madelung energy term has to be added to the total binding energy change:

$$\Delta W'_{M} = \mu'_{Ba}(6 - q_{Ba}) + \mu'_{O}(6 - q_{O}) = \ldots = -6\tilde{w}_0 Q(T_{2k} + T_{2k+1}) + \tilde{w}_0 Q^2 T_{2k+1} + \tilde{w}_0 Q x \Delta T \quad (20)$$

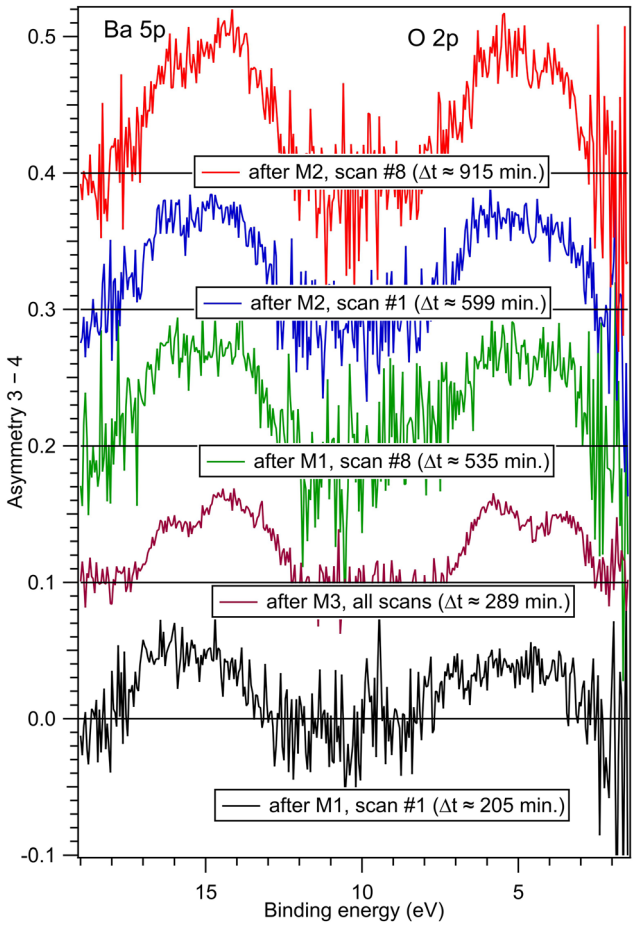

Fig. 6 Time evolution of the recorded spin asymmetry between spin channels 3 and 4 during individual scans (46 min each) together with the corresponding signal of the M3 experiment. For each signal, an estimate of the time elapsed from the end of the sample preparation is given.

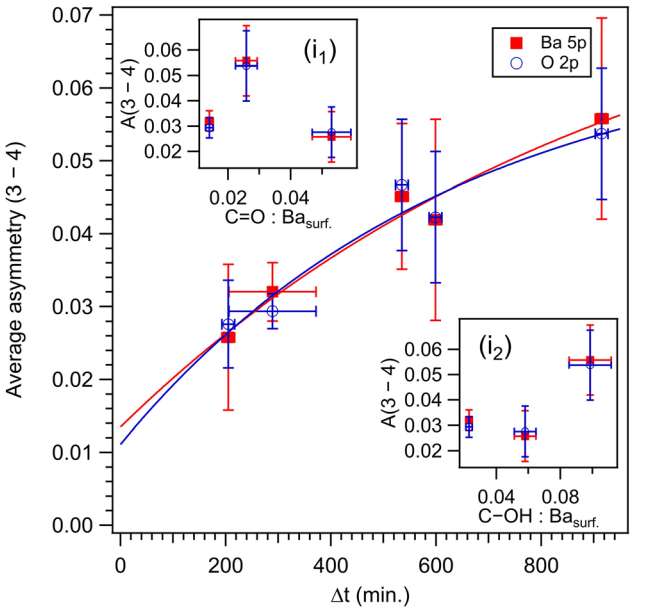

Fig. 7 Average asymmetries between 3–4 spin channels represented as a function of the time elapsed from the sample preparation, together with a fit with an exponentially saturating function. The inserts are plots of the asymmetry signals *vs.* the amount of the two main sample contamination: C 1s higher binding energy for (i_1) and C 1s lowest binding energy for (i_2).

with $\Delta T = T_{2k} - T_{2k+1} \approx 0.0104$. Adding this energy to eqn (16) modifies $B(Q)$, such that now the maximum binding energy change is obtained for:

$$x_{\max.} = \frac{Q}{2} + \frac{\tilde{w}_0 Q \Delta T}{4(\tilde{w}_0 \Delta S + w)} \approx 0.512Q \qquad (21)$$

by using the values estimated above. Also, the free term from eqn (16) reads now:

$$C(Q) = 6\tilde{w}_0 Q(S_{2k} + S_{2k+1} - T_{2k} - T_{2k+1}) + \tilde{w}_0 Q^2(T_{2k+1} - S_{2k}) + wQ(6 - Q) \qquad (22)$$

and it was numerically checked that neither of $(S_{2k} + S_{2k+1} - T_{2k} - T_{2k+1})$ nor $(T_{2k+1} - S_{2k})$ diverge when increasing the limit of the summation.

Variation of the spin asymmetry signal: possible effects of contamination

It is readily observed from Fig. 4 that the spin asymmetry signal increases for the M2 experiment. One possible explanation relies on the progressive changes of sample contamination: it is demonstrated that after the spin-resolved M1, 2 experiment the amount of C=O contamination decreases (from ~0.053 to ~0.026), whereas the amount of C–OH increases (from ~0.058 to ~0.099; compare Fig. 2 and Table 2 with Fig. S3 and Table S1 from the SI). We might connect the presence of contaminants to some changes of surface charging of the outermost BaO layer: C=O is expected to donate electrons to the surface, decreasing the positive charge state of surface barium and oxygen, whereas C–OH-like moieties might trap electrons from the surface, increasing the positive charge state of surface BaO. Therefore, a decrease in the C=O content and increase of the C–OH implies more holes in the surface layer and therefore an increased spin moment. But this hypothesis is contradicted by the M3 experiment, where the contamination was lower and, despite this fact, the spin asymmetry is lower than for M2. Even by analyzing the difference in contamination between C–OH and C=O (~0.005 for M1, ~0.07 for M2 and ~0.09 for M3) one cannot explain the variation of the observed asymmetry.

To gain more insight in this phenomenon, Fig. 6 represents 3–4 asymmetries obtained from individual spin-resolved scans recorded during the M1, 2 experiment (we note that the signals represented in Fig. 4 are sums of eight scans, each one lasting ~46 minutes) together with the 3–4 asymmetry obtained from the M3 experiment, ordered by the average time elapsed from the sample preparation Δt. A progressive increase in time of the signal is clear. Also, the first scan after the M2 magnetization is quite similar to the last scan after the M1 magnetization. The obtained average asymmetries between 3–4 channels are represented *vs.* Δt in Fig. 7, with error bars estimated in the most pessimistic scenario: half of the total acquisition time for a scan, maximum error in computing the average asymmetry,

mainly related to the ambiguity of defining the region of interest for integration of a spectrum. The increase of the signal in time seems to be non-linear, but rather described by a saturating function $a-b\ \exp(-t/\tau)$, with τ ranging between 635 min for the O 2p asymmetry and 967 min for the Ba 5p asymmetry. The insets in Fig. 7 represent the evolution of the asymmetry signal plotted as a function of the sample contamination derived from the closest XPS series of scans: just before the M1 magnetization for the first scan of the M1 experiment, just after the M1 + M2 spin-resolved measurements for the last scan of the M2 experiment, and just before the M3 experiment for the corresponding asymmetry. Although such representation is not 100% rigorous, it allows one to derive that there is no monotonous dependence of the spin asymmetry on the contamination level. The asymmetry obtained for the M3 experiment, with contamination level significantly lower than before M1 is slightly higher than the asymmetry of the first M1 scan, but lower than that of the last M1 scan.

Hence, one should find another explanation for the time variation of the observed asymmetries. One possible explanation might be related to the sample temperature. Some details of the experiments need to be taken into account for understanding this behavior and are described in greater detail in the SI (S5). The main supposition will be that the cooling down of the sample surface towards the room temperature is quite slow and might last more than ten hours, no matter which is the indication of the manipulator's thermocouple, which is placed at about 1 cm from the sample surface. There are multiple reasons for this slow cooling: the thermal contact between the sample holder and the body of the manipulator and the thermal contact between the sample itself and the sample holder are not perfect, not to speak about the limited thermal conductivity of the Nb:$SrTiO_3$(001) substrate. This slow cooling is well known in the community of surface scientists: for instance, in the case of a GaAs(001) single crystal mounted in a similar setup, one needed to wait about 12 hours for cooling down near the room temperature without cooling the manipulator with liquid nitrogen, and about half of this time when the manipulator was cooled down by a liquid nitrogen flux.[30] Therefore, it is reasonable to suppose that the transition temperature of the $BaTiO_3$(001) surface is not very high and that during the scans after the M1 and M3 experiments, the sample temperature was more elevated than for the M2 experiment. The exponential saturation of the asymmetry signal as a function of time seems to confirm this hypothesis but, nevertheless, new experiments with precise measurement of the surface temperature are needed for a complete description of the temperature dependence of the spin asymmetry.

An exercise taking seriously the exponential saturation function is to use the asymptotic asymmetries of 0.082 ± 0.023 for Ba and 0.067 ± 0.014 for O. In this case the charges derived by using $q = 6A/(1 + A)$ are $(0.45 \pm 0.12)e$ for barium and $(0.38 \pm 0.07)e$ for oxygen. The barium charge represents about 55% of the total charge accumulated on a BaO unit cell.

Back to contamination as a possible origin of the spin asymmetry, of the about 14% total amount of surface carbon as related to a surface BaO unit cell, only about 8.6% represents carbon which might be susceptible to binding with surface oxygen atoms. In the most drastic case which might be imagined for affecting the surface electronic states, each of these carbon atoms is bound to surface oxygen from the first monolayer. Assuming, again in the most severe case, that each such bond is accompanied by one elementary charge transferred from carbon to oxygen, this makes at most about −0.09e additional charge for each surface oxygen. But the (ferroelectric induced) surface charge inferred for each surface BaO unit cell from spin-resolved measurements was between +0.3e and +0.4e (or even $\sim$ 0.8e if one considers the asymptotic values from the exponential fits from Fig. 7). If we should introduce also the charge (negative, maximal in absolute value) transferred due to bonds with contaminating layers, then the effect of surface positive charge accumulation due to ferroelectricity for an absolutely clean surface would be further reinforced by at most $20 \pm 3\%$. Hence, the main findings of this work should be still valid and even reinforced in the case of an absolutely clean surface. In particular, the existence of some holes in Ba 5d states should not be influenced by the tiny number of carbonaceous compounds identified by surface sensitive XPS.

Note that such a tiny amount of carbon contamination would be barely visible by using a standard XPS method with a laboratory source. The ratio between cross sections of Ba 4d and C 1s is about 1.78 at a photon energy of 390 eV[20] and in the actual case, experimentally, the area ratio $C_{C=O+C-O-C}$:$Ba_{surf.}$ $\approx$ 7.9%. When using a conventional XPS with Al K_α excitation (1486.7 eV), the ratio of the cross sections is about 5.9, *i.e.* about 3.3 times lower. Also, in standard XPS there is little hope to derive separately the Ba 4d surface component; instead, the whole Ba 4d signal will be recorded, which would be the equivalent of about 5–6 BaO layers (inelastic mean free path on the order of at least 2 nm). Additionally, the width of the Ba 4d surface component should be in the range of the experimental linewidth of a standard monochromated XPS machine ($\sim$1 eV), while all involved C 1s structures extend over a spectral range of about 5 eV. As a consequence, with a conventional XPS the intensity ratio between the C 1 and the Ba 4d lines would be in the range of $0.079/(5 \times 3.3 \times 10) \approx 0.05\%$. This last evaluation was made in order to prove that the possible sample contamination was properly taken into account in this work by performing XPS in a high surface sensitive mode and to offer some figures to be compared with other investigations using standard XPS.

Surface multiferroicity of (001)BaO-terminated barium titanate: considerations on possible magnetoelectric effects

We may then assume that the terminal BaO three layers of $BaTiO_3$(001) features multiferroicity, *i.e.* simultaneous ferromagnetic and ferroelectric ordering, both originating from the surface electronic reconstruction. The main origin of this is the ferroelectricity of the material: a permanent ferroelectric polarization has been found to be dictated by the interface with the substrate,[16] since the workfunction of $BaTiO_3$ is about 4.8 eV[31] and that of Nb:$SrTiO_3$(001) is lower than 4.2 eV.[16] Ferroelectric dipoles

are derived from the rumpling of atomic layers, in particular the displacement of positive ions (especially titanium) in the direction of the polarization and of negative oxygen in the direction opposite to the polarization. It was found by photoelectron diffraction that the rumpling of surface layers is quenched,[27] but in order to preserve a dipole moment at the last atomic layers an electronic reconstruction is needed, in particular one should suppose that the last atomic layer is positively charged. This is clearly manifested as the shift towards a higher binding energy of surface components of barium and oxygen. This shift can also be ascribed to a lack of presence of surrounding positive ions, since similar surface components are visible also in SrO-terminated $SrTiO_3$(001). But a detailed analysis of the O 1s surface core level shift yields values of $\sim$1.09 eV for $SrTiO_3$(001)[7] and $\sim$1.26 eV for $BaTiO_3$(001) (see Table 2). The additional chemical shift of $\sim$0.17 eV is in line with an extra oxygen positive charge state of up to 0.2 eV.

The overall charge state inferred for a BaO surface unit cell with lattice parameter a = 3.905 Å is $(0.274 \pm 0.047)e$ for the M1 experiment and $(0.445 \pm 0.066)e$ for the M2 experiment, which yields a surface charge density (one has to divide by a^2) of 0.288 ± 0.050 C m^{-2} and 0.467 ± 0.069 C m^{-2}, respectively. The first value is in line with the reported polarization of barium titanate thin films.[32]

Out of many possible origins of multiferroicity,[33] electronic reconstruction and surface charging are not very often taken into considerations. Apart for the previous work on $SrTiO_3$(001)[7] and especially on $SrTiO_3$(011),[8] similar results connecting surface charging with spin imbalance were obtained on Pt(001)–hex.[17] However, in order to exploit the multiferroicity, one needs to be able to vary either the polarization of the magnetization of the material. Some hopes are offered by this work, since a different magnetization procedure yielded a different value of q_{Ba}, q_O and Q. Differences might be ascribed also to the formation of some ferroelectric/ferromagnetic domains, but repeated experiments revealed that a so thin $BaTiO_3$(001) film remains in a single domain ferroelectric state due to the self-doping mechanism able to generate additional electrons for "compensation" or "stabilization".[34] At the same time, the formation of ferromagnetic domains for a so thin film was shown to be unlikely by a modified Kittel theory which takes into account the film thickness.[35]

Also, inspecting by XPS the sample after the second (M2) magnetization procedure yielded no consistent differences in binding energies or surface core level shifts with respect to the data just presented, recorded before the magnetization procedures. A similar experiment is planned for the future, with more accurate control of the applied magnetic field. At this point, we cannot comment more on the possibility of varying the electric polarization by the applied magnetic field. The converse magnetoelectric process, *i.e.* varying the magnetization by an applied electric field is hard to be imagined, since the phenomenon we report is intrinsically connected to the free BaO surface of (001) barium titanate grown on niobium-doped strontium titanate. At the same point, there are also some fundamental limitations in exploiting magnetoelectric effects for such systems where the spin imbalance originates from incomplete valence shells, as outlined below.

Actually, the polarization is oriented along the [001] axis (normal to the surface and is dictated by the in-plane strain due to the STON(001) substrate and to the lower $BaTiO_3$(001) film thickness, yielding the octahedral distortion and the preferred axis for polarization. The magnetization should lie in-plane due to the demagnetization field.[36] The experiments presented in this work suggested that the in-plane easy magnetization axis should be [100] (Fig. 3(d)).

Any considerations based on the linear magnetoelectric effect considerations cannot be applied immediately in the case of systems with strong permanent electric or magnetic moments. Moreover, a so thin layer which exhibits single domain ferroelectric and ferromagnetic structure[34–36] is expected to have almost rectangular hysteresis cycles. Reversing the magnetization by an applied field does not necessarily yield to a reversal of the orientation of the ferroelectric polarization, since this is imposed by the interface with the substrate.[16] Thus, it is hard to imagine an experiment where the reversal of the polarization could be induced by an applied magnetic field and we specified above that, since the multiferroicity is particular to the surface BaO layer, unaffected by any contacts, adsorbates (*etc.*), one cannot imagine the way one might apply an electric field on this system.

5. Conclusions

This work reinforced the evidence of magnetism occurring on a surface layer due to incomplete occupation of densities of states induced by surface electronic reconstruction, as in $SrTiO_3$(011).[8] A first novelty here is the ferroelectricity of the material; as such, this is one of the few known examples of a possible multiferroic (2D) surface. A second novelty is related to the fact that the charge depletion occurs on both O 2p (last occupied states) and deeper Ba 5p states. Thus, both densities of states feature detectable spin asymmetry. A simple energetic model was proposed, by taking into consideration chemical shifts due to ionization and crystal field effects, and the result is that the extra surface charge should be (almost) evenly distributed on surface barium and oxygen, in line with the observed spin asymmetries (within 12% relative deviation). The diagram of occupied electronic states features some kind of permanent population inversion (holes in the Ba 5p density of states, with O 2p occupied states at higher energy). The detected increase in time of the spin asymmetry signal is most probably due to the cooling down of the sample surface during the measurements, as expected for any magnetic system with Curie temperature not far away from room temperature.

Ethics declarations

All authors have made substantial contributions to the following: (1) the conception and design of the study, the acquisition

of data, or the analysis and interpretation of data; (2) drafting the article or critically revising its important intellectual content; and (3) final approval of the version submitted. All authors and responsible authorities where the work was carried out have approved this publication. All authors disclose any financial or other interests related to the submitted work that (1) could affect or have the perception of affecting the author's objectivity, or (2) could influence or have the perception of influencing the content of the article. All authors and their immediate family members disclose any personal financial interests (*e.g.* stocks or shares in companies with interests related to the submitted work or consulting fees from companies that could have interests related to the work), professional affiliations, advisory positions, board memberships, or patent holdings that are related to the subject matter of this contribution.

Author contributions

Larisa E. Borcan: investigation, writing – review & editing, Alexandru-Cristi Iancu: investigation, writing – review & editing, Nicoleta G. Apostol: investigation, writing – review & editing, Adela Nicolaev: investigation, writing – review & editing, Cristian M. Teodorescu: conceptualization, supervision, investigation, validation, formal analysis, software, visualization, methodology, theoretical aspects, writing – original draft, writing – review & editing, funding acquisition, project administration.

Conflicts of interest

There are no conflicts to declare.

Data availability

All data and resulting analyses are conveniently presented in the manuscript. Numeric values and the data analysis can be made available on request from the corresponding author in form of Igor Pro files, including the data analysis and graphics.

Supplementary information (SI): S1 Magnetization geometry, experiments M1, M2. S2 Magnetization geometry, experiment M3. S3 XPS data recorded after spin-resolved measurements (M1 + M2). S4 XPS data recorded before the third experiment (M3). S5 Spin-resolved measurements, third experiment (M3). See DOI: **https://doi.org/10.1039/d5ma00363f**.

Acknowledgements

The $BaTiO_3$(001) thin film was prepared by Dr Cristina F. Chirilă. XRD characterization studies were performed by Dr Dana G. Popescu. The coil for *in situ* ample magnetization (M3 experiment) was installed and calibrated by Dr Marco Bianchi. This work was funded by the Core Program of the National Institute of Materials Physics, under the project PC2–PN23080202. All experiments were performed using the National Interest Setup "System of complex XPS/ESCA installations and research using synchrotron radiation".

References

1 N. Sharma, A. Gaur and U. K. Gaur, Multiferroic behavior of nanocrystalline BaTiO3 sintered at different temperatures, *Ceram. Int.*, 2014, **40**, 16441–16448.
2 W. L. Zhou, H. M. Deng, N. F. Ding, L. Yu, F. Y. Yue, P. X. Yang and J. H. Chu, Microstructure tuning and magnetism switching of ferroelectric barium titanate, *Mater. Charact.*, 2015, **107**, 1–6.
3 R. V. K. Mangalam, N. Ray, U. V. Waghmare, A. Sundaresana and C. N. R. Rao, Multiferroic properties of nanocrystalline $BaTiO_3$, *Solid State Commun.*, 2009, **149**, 1–5.
4 L. N. Korotkov, N. A. Tolstykh, T. N. Korotkova, N. A. Emelianov, R. M. Eremina, R. G. Batulin, M. A. Cherosov and F. D. Al' Jaafari, Influence of oxygen vacancies on magnetic and dielectric properties of nanocrystaline barium titanate, *Ferroelectrics*, 2020, **567**, 264–270.
5 S. Ramakanth and K. C. James Raju, Charge transfer induced magnetism in sol–gel derived nanocrystalline $BaTiO_3$, *Solid State Commun.*, 2014, **187**, 59–63.
6 S. B. Qin, D. Liu, Z. Y. Zuo, Y. H. Song, X. L. Zhang, F. F. Zheng, H. Liu and X.-G. Xu, UV-Irradiation-Enhanced Ferromagnetism in $BaTiO_3$, *J. Phys. Chem. Lett.*, 2010, **1**, 238–241.
7 D. G. Popescu, A. Nicolaev, R. M. Costescu, L. E. Borcan, G. A. Lungu, C. A. Tache, M. A. Huşanu and C. M. Teodorescu, Spin asymmetry of O 2p –related states in $SrTiO_3$(001), *Phys. Scr.*, 2024, **99**, 105925(1–11).
8 L. E. Borcan, A.-C. Iancu, D. G. Popescu and C. M. Teodorescu, Considerable spin asymmetry of deep valence states induced by partial neutralization of charged $SrTiO_3$(011) surfaces, *J. Chem. Phys.*, 2025, **162**, 054707(1–13).
9 P. W. Tasker, The stability of ionic crystal surfaces, *J. Phys. C: Solid State Phys.*, 1979, **12**, 4977–4984.
10 J. Osterwalder, Spin-polarized photoemission, *Lect. Notes Phys.*, 2006, **697**, 95–120.
11 A.-C. Iancu, N. G. Apostol, A. Nicolaev, L. E. Abramiuc, C. F. Chirilă, D. G. Popescu and C. M. Teodorescu, Molecular adsorption–desorption of carbon monoxide on ferroelectric $BaTiO_3$(001), *Mater. Adv.*, 2024, **5**, 5709–5723.
12 A.-C. Iancu, G. A. Lungu, C. A. Tache and C. M. Teodorescu, Ferroelectric-enabled significant carbon dioxide molecular adsorption on $BaTiO_3$(001), *Mater. Adv.*, 2024, **5**, 8798–8811.
13 A.-C. Iancu, A. Nicolaev, N. G. Apostol, L. E. Abramiuc and C. M. Teodorescu, Reversible oxidation of ethylene on ferroelectric $BaTiO_3$(001): an X-ray photoelectron spectroscopy study, *Heliyon*, 2024, **10**, e35072(1–14).
14 N. G. Apostol, L. E. Stoflea, G. A. Lungu, C. Chirila, L. Trupina, R. F. Negrea, C. Ghica, L. Pintilie and C. M. Teodorescu, Charge transfer and band bending at Au/Pb(Zr,Ti)O_3 interfaces investigated by photoelectron spectroscopy, *Appl. Surf. Sci.*, 2013, **273**, 415–425.
15 L. E. Ştoflea, N. G. Apostol, L. Trupină and C. M. Teodorescu, Selective adsorption of contaminants on Pb(Zr,Ti)O_3 surfaces shown by X-ray photoelectron spectroscopy, *J. Mater. Chem. A*, 2014, **2**, 14386–14392.

16 L. C. Tănase, L. E. Abramiuc, D. G. Popescu, A.-M. Trandafir, N. G. Apostol, I. C. Bucur, L. Hrib, L. Pintilie, I. Pasuk, L. Trupină and C. M. Teodorescu, Polarization orientation in lead zirconate titanate (001) thin films driven by the interface with the substrate, *Phys. Rev. Appl.*, 2018, **10**, 034020(1–19).
17 L. E. Borcan, C. M. Teodorescu, A.-C. Iancu, N. G. Apostol, A. Nicolaev, R. M. Costescu, M. A. Huşanu, D. G. Popescu, G. A. Lungu and M. Bianchi, Surface spin asymmetry in Pt(001)–hex induced by electron accumulation, *J. Phys.: Mater.*, 2024, **8**, 035010(1–35).
18 https://www.specs-group.com/fileadmin/user_upload/products/application-notes /ANote Mott_Detector_for_PHOIBOS.pdf.
19 M. Henzler, LEED from epitaxial surfaces, *Surf. Sci.*, 1993, **298**, 369–377.
20 J. J. Yeh and I. Lindau, Atomic subshell photoionization cross sections and asymmetry parameters: $1 \leq Z \leq 103$, *At. Data Nucl. Data Tables*, 1985, **32**, 1–155See also.
21 M. Iliut, C. Leordean, V. Canpean, C. M. Teodorescu and S. Astilean, A new green, ascorbic acid-assisted method for versatile synthesis of Au-graphene hybrids as efficient surface-enhanced Raman scattering platforms, *J. Mater. Chem. C*, 2013, **1**, 4094–4104.
22 C. M. Teodorescu, J. M. Esteva and R. C. Karnatak, and A. El Afif, An approximation of the Voigt I profile for the fitting of experimental x-ray absorption data, *Nucl. Instrum. Methods Phys. Res.*, 1994, **345**, 141–147.
23 D. Luca, C. M. Teodorescu, R. Apetrei, D. Macovei and D. Mardare, Preparation and characterization of increased-efficiency photocatalytic $TiO_{2-2x}N_x$ thin films, *Thin Solid Films*, 2017, **515**, 8605–8610.
24 D. Mardare, D. Luca, C. M. Teodorescu and D. Macovei, On the hydrophilicity of nitrogen-doped TiO_2 thin films, *Surf. Sci.*, 2007, **601**, 4515–4520.
25 C. M. Teodorescu, Ferroelectricity in thin films driven by charges accumulated at interfaces, *Phys. Chem. Chem. Phys.*, 2021, **23**, 4085–4093.
26 I. Derkaoui, M. Achehboune, I. Boukhoubza, Z. El Adnani and A. Rezzouk, Improved first-principles electronic band structure for cubic (Pm3m) and tetragonal (P4mm, P4/mmm) phases of $BaTiO_3$ using the Hubbard U correction, *Comput. Mater. Sci.*, 2023, **217**, 111913(1–9).
27 A. Pancotti, J. Wang, P. Chen, L. Tortech, C. M. Teodorescu, E. Frantzeskakis and N. Barrett, X-ray photoelectron diffraction study of relaxation and rumpling of ferroelectric domains in $BaTiO_3$(001), *Phys. Rev. B*, 2013, **87**, 184116(1–10).
28 L. Pintilie and M. Alexe, Metal-ferroelectric-metal heterostructures with Schottky contacts. Influence of the ferroelectric properties, *J. Appl. Phys.*, 2005, **98**, 124103(1–8).
29 R. D. Shannon, Revised effective ionic radii and systematic studies of interatomic distances in halides and chalcogenides, *Acta Crystallogr., Sect. A*, 1976, **32**, 751–767.
30 C. M. Teodorescu and D. Luca, Comparative study of magnetism and interface composition in Fe/GaAs(100) and Fe/InAs(100), *Surf. Sci.*, 2006, **600**, 4200–4204.
31 D. G. Popescu, M. A. Husanu, C. Chirila, L. Pintilie and C. M. Teodorescu, The interplay of work function and polarization state at the Schottky barriers height for Cu/$BaTiO_3$ interface, *Appl. Surf. Sci.*, 2020, **502**, 144101(1–7).
32 I. Pintilie, C. M. Teodorescu, C. Ghica, C. Chirila, A. G. Boni, L. Hrib, I. Pasuk, R. Negrea, N. G. Apostol and L. Pintilie, Polarization-control of the potential barrier at the electrode interfaces in epitaxial ferroelectric thin films, *ACS Appl. Mater. Interfaces*, 2014, **6**, 2929–2939.
33 M. Fiebig, Revival of the magnetoelectric effect, *J. Phys. D: Appl. Phys.*, 2005, **38**, R123–R152.
34 L. Pintilie, C. Ghica, C. M. Teodorescu, I. Pintilie, C. Chirila, I. Pasuk, L. Trupina, L. Hrib, A. G. Boni, N. G. Apostol, L. E. Abramiuc, R. Negrea, M. Stefan and D. Ghica, Polarization induced self-doping in epitaxial $Pb(Zr_{0.20}Ti_{0.80})O_3$ thin films, *Sci. Rep.*, 2015, **5**, 14974(1–14).
35 C. M. Teodorescu, Kittel's model for ferromagnetic domains, revised and completed, including the derivation of the magnetic hysteresis, *Results Phys.*, 2023, **46**, 106287(1–17).
36 C. M. Teodorescu, Two dimensional landscape of ferromagnetic domains and the resulting magnetization curves, *Results Phys.*, 2023, **54**, 107109.